



四川盆地须家河组诺利—瑞替期之交气候变迁及其驱动机制

陈俞超, 金鑫, 杜怡星, 张云望, 李滨兵, 时志强

引用本文:

陈俞超, 金鑫, 杜怡星, 张云望, 李滨兵, 时志强. 四川盆地须家河组诺利—瑞替期之交气候变迁及其驱动机制[J]. 沉积学报, 2024, 42(4): 1212–1228.

CHEN YuChao, JIN Xin, DU YiXing, et al. Paleoclimate Perturbation and Its Driving Mechanism Across Norian–Rhaetian Transition (Late Triassic) in the Xujiahe Formation, Sichuan Basin[J]. *Acta Sedimentologica Sinica*, 2024, 42(4): 1212–1228.

相似文章推荐（请使用火狐或IE浏览器查看文章）

Similar articles recommended (Please use Firefox or IE to view the article)

[古近纪气候变化在东海盆地内的化石记录](#)

Sedimentary Response to Paleoclimate Change in the East China Sea Shelf Basin

沉积学报. 2019, 37(2): 320–329 <https://doi.org/10.14027/j.issn.1000-0550.2018.133>

[柴西上干柴沟组中上段介壳微量元素古环境古气候意义](#)

Paleoenvironmental and Paleoclimatic Significance of Trace Elements in Ostracod Shells in the Upper?Middle Section, Upper Ganchaigou Formation, Western Qaidam Basin

沉积学报. 2019, 37(5): 992–1005 <https://doi.org/10.14027/j.issn.1000-0550.2018.192>

[四川宣汉七里峡T3x/T2l界线沉积环境演化分析](#)

The Analysis of Sedimentary Environmental Evolution of the T3x/T2l Boundary Transition in Qilixia of Xuanhan, Sichuan

沉积学报. 2015, 33(6): 1149–1158 <https://doi.org/10.14027/j.cnki.cjxb.2015.06.008>

[川北南江地区下三叠统飞一段风暴沉积特征及地质意义](#)

The Sedimentary Characteristics and Geological Significances of Carbonate Tempestites near the Boundary of Late Permian to Early Triassic at Nanjiang Section, North of Sichuan Basin

沉积学报. 2015, 33(5): 899–908 <https://doi.org/10.14027/j.cnki.cjxb.2015.05.006>

[南雄盆地晚白垩世—古新世陆源沉积组份变化的古气候指示](#)

Paleoclimate Indication of Terrigenous Clastic Rock's Component during the Late Cretaceous–Early Paleocene in the Nanxiong Basin

沉积学报. 2015, 33(1): 116–123 <https://doi.org/10.14027/j.cnki.cjxb.2015.01.012>

文章编号:1000-0550(2024)04-1212-17

DOI: 10.14027/j.issn.1000-0550.2022.147

四川盆地须家河组诺利—瑞替期之交气候变迁及其驱动机制

陈俞超¹, 金鑫^{1,2,3}, 杜怡星^{1,2}, 张云望¹, 李滨兵¹, 时志强^{1,2}

1. 成都理工大学沉积地质研究院, 成都 610059

2. 油气藏地质及开发工程国家重点实验室(成都理工大学), 成都 610059

3. 中国科学院地球环境研究所黄土与第四纪地质国家重点实验室, 西安 710061

摘要 【目的】晚三叠世诺利—瑞替期之交(Norian-Rhaetian Transition, NRT)的古气候—环境发生了显著的变化,且伴随着全球性的碳同位素负漂和生物绝灭事件。目前多数NRT研究均聚焦于特提斯域的浅海相地层,而关于NRT时期陆地的气候与环境变迁及其驱动机制的研究还非常缺乏。【方法】为了解决这一科学问题,对四川盆地西北部以河流相和沼泽相沉积为主的诺利—瑞替阶剖面(须家河剖面)进行研究。利用主、微量元素分析,重建了四川盆地须家河组NRT时期的古气候演化过程并探讨了其驱动机制。【结果】须家河组诺利末期(剖面:105.5~129.5 m)古气候指数CIA、Rb/Sr相对较高,R值相对较低(平均值分别为73、1.2、8.2);诺利—瑞替期界线处(剖面:129.5~135 m)CIA、Rb/Sr相对较低,R值相对较高(平均值分别为61、0.5、13.5)。【结论】四川盆地须家河组NRT时期气候波动频繁,诺利末期以温暖湿润的气候为主,到了诺利—瑞替期界线附近,发生了一次短暂的降温事件。须家河组NRT时期温暖—干冷的古气候变化和诺利—瑞替期界线处的降温事件主要受到晚三叠世盛行于泛大陆中的超级季风控制,但不排除同时期的火山活动和野火事件对古气候系统的影响,然而火山活动、野火事件以及气候环境变化三者间的互馈机制,需要进一步明晰。

关键词 晚三叠世; 须家河组; 古气候; 风化指数; 四川盆地

第一作者简介 陈俞超,男,1997年出生,硕士研究生,沉积地球化学,E-mail: qwecyc1010@163.com

通信作者 金鑫,男,副教授,E-mail: jinxin2012cdut@163.com

中图分类号 P532 **文献标志码** A

0 引言

在晚三叠世诺利—瑞替期之交(Norian-Rhaetian transition, NRT),古环境发生了显著变化^[1-2],同时生物灭绝和更替也更加频繁^[3-4]。然而,NRT时期生物灭绝和更替的原因仍然具有争议^[4-6]。同时期的火山活动(如Angayucham大火成岩省爆发)被认为是导致NRT时期生物灭绝的主要原因^[2,4],大规模的火山活动释放的大量温室气体,会导致全球温度上升,甚至出现极端气候,最终可能导致NRT时期的生物危机^[7-10]。

上述观点主要来自于NRT时期的海相地层记录,却极少涉及陆相地层。研究表明陆相地层也能够有效记录地质事件过程中的古气候—环境变迁,

如二叠纪末生物大灭绝事件^[11]。四川盆地位于中国西南地区,发育了上三叠统—第四系陆相地层^[12],其中上三叠统须家河组发育连续的诺利—瑞替阶地层^[2,13]。此外,四川盆地记录到了诺利—瑞替期有机碳同位素的多期次波动和汞(Hg)元素的浓度异常,表明四川盆地在此时期可能受到火山作用影响,并导致古气候—环境发生了明显变化^[2]。然而,前人对四川盆地须家河组诺利—瑞替期的古气候重建工作主要集中于古植物、沉积学研究和碳同位素研究^[2-3,14-16],而缺乏元素地球化学证据,从而限制了对四川盆地NRT时期气候变化的精确认识以及不同研究方法之间的相互比较。

本文以四川盆地须家河剖面为研究对象,对研究剖面的须家河组岩石样品进行了主微量元素分析,并

收稿日期:2022-08-24;修回日期:2022-11-16;录用日期:2022-11-24;网络出版日期:2022-11-24

基金项目:中国科学院地球环境研究所黄土与第四系地质国家重点实验室开放基金(SKLLQGZR2005)[Foundation: State Key Laboratory of Loess and Quaternary Geology, Institute of Earth Environment, Chinese Academy of Sciences, No. SKLLQGZR2005]

利用相关元素地球化学指标,重建了四川盆地NRT时期的古气候记录,并讨论了其可能的驱动机制,为探讨NRT时期生物灭绝和更替的原因提供启示。

1 地质背景

四川盆地位于华南板块西北部,是大型的陆相含油气盆地^[17-18]。盆地内发育一套元古代至中三叠世的海相碳酸盐岩^[19],上覆上三叠统至第四系陆相地层^[12]。中三叠统与上三叠统之间的不整合,标志着华南板块西缘逐步由被动大陆边缘向前陆盆地转换^[19],地势由西高东低变为东高西低,海水从盆地西缘退出,碳酸盐岩台地阶段结束^[20-21]。四川盆地在晚三叠世时期处于特提斯东缘^[22],而现在盆地东面和南面为滇黔川鄂台褶带,西面为松潘—甘孜褶皱带和龙门山断褶带,北面为米仓山隆起和秦岭断褶系^[23](图1)。

四川盆地上三叠统发育马鞍塘组、小塘子组和须家河组。有学者将小塘子组等同于须家河组一段^[17,24],主要由砂岩和泥岩夹层为主的河流相、湖泊相和沼泽相地层组成^[17]。前人对须家河组的划分提

出过多种不同的方案,最少的将其划分为四段,最多的则将其划分为七段^[25-27]。本文使用夏宗实等^[28]采用的地层划分方案,自下而上将须家河组分为须一段至须六段,其中须一段、须三段、须五段以灰色泥岩为主,伴有丰富的植物化石和煤层,沉积相主要为湖泊相或沼泽相;须二段、须四段、须六段以粗粒砂岩为主,沉积相主要为河流相^[18]。

此次研究的须家河剖面,位于广元市东北方向4.5 km处的须家河村(图1)。剖面的~110.8 m至~115 m、~118.6 m至~120.6 m为泥灰质粉砂岩,~104.4 m至~106.5 m、~114.9 m至~118.6 m为细砂岩,块状粗砂岩主要位于~124.2 m至~137.5 m^[2],见图2^[2,4,13-14,29]。同时剖面中识别出两套煤层,分别为M1、M2;其中M1位于~104.4 m处,M2位于~123.5 m处,两者厚度约为10 cm。基于黑碳研究,发现M2记录有低温成因的古野火事件^[2](图2)。Jin et al.^[2]还识别出至少四次有机碳同位素负漂并能够进行全球对比以及三次汞元素富集的层位(图2)。Jin et al.^[2]认为须家河剖面中碳同位素负漂和汞元素富集可能与同时期的Angayucham大火成岩省爆发有关,但不排除区域长英质火山活动的影响。

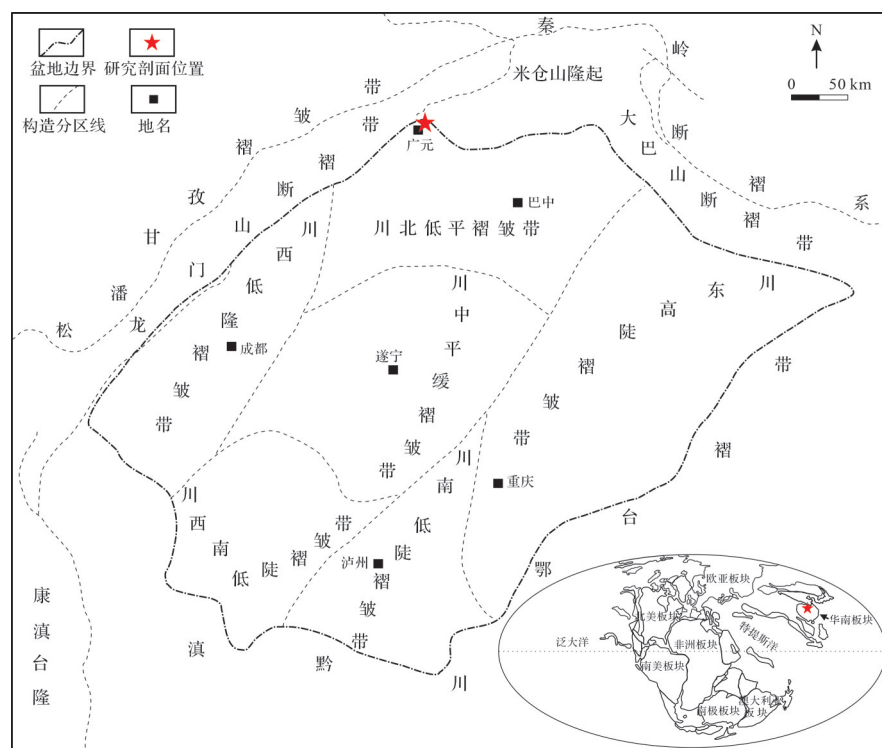


图1 四川盆地构造简图及诺利期全球古地理图

诺利期古地理图据文献[22]修改;四川盆地构造简图据文献[23]修改;图中红色五角星代表研究剖面位置

Fig.1 Map showing the tectonic background of the Sichuan Basin and general paleogeography of the Norian

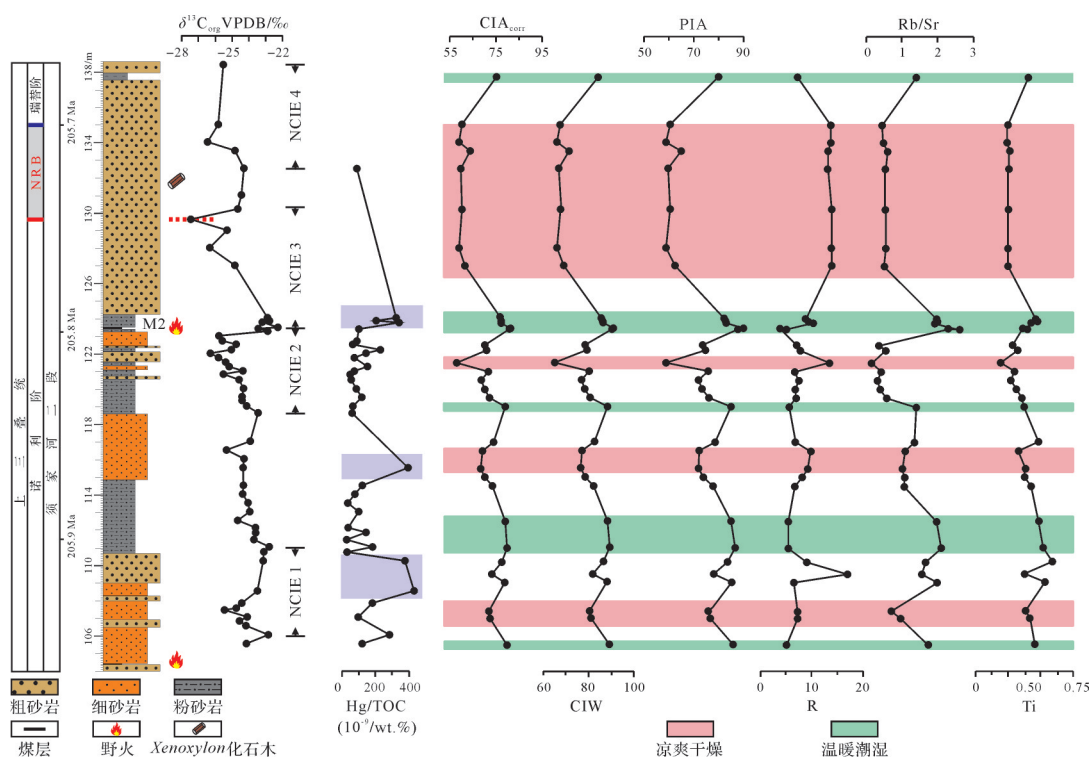


图2 四川盆地须家河组诺利—瑞替期之交地球化学指标在地层垂向上的变化

蓝色实线为 Li et al.^[13]和 Maron et al.^[29]根据磁性地层学、碳同位素以及牙形石厘定的 NRB; 红色实线为 Jin et al.^[2]和 Rigo et al.^[14]根据碳同位素厘定的 NRB; 蓝色实线与红色实线之间的灰色区域为 NRB 的不确定区间; $\delta^{13}\text{C}_{\text{org}}$ VPDB/Hg/TOC、地质年龄、地层岩性及古野火信息据 Jin et al.^[2]; Xenoxyylon 化石木及其大致层位据 Tian et al.^[14]; 其中, 淡蓝色方块为汞浓度异常层位, NCIE, 碳同位素负漂

Fig.2 Change of geochemical proxies in stratigraphic order across the Norian-Rhaetian transition in the Xujiuhe Formation, Sichuan Basin

2 诺利—瑞替阶界线(Norian - Rhaetian Boundary, NRB)研究

瑞替期持续的时间一直存在争议, 有长瑞替期和短瑞替期两种观点^[30-32], 这种差异在很大程度上是由 NRB 的生物地层标准的不同所引起的^[32]。短瑞替期持续时间为~4 Myr, 其底界以牙形石 *Mi. posthermannsteini* sensu stricto 首现为标志^[30-32]。诺利—瑞替阶的生物地层标准可与 Newark 盆地磁极性序列(国际标准磁极性序列)相对应, 得出瑞替阶底界为 205.7 Ma^[30-31](即短瑞替期)。此外, Maron et al.^[29]还在意大利 Pignola-Abriola 剖面中提出了一个化学地层标准(即 NRB 处存在一个 $\delta^{13}\text{C}_{\text{org}}$ 负漂, 偏移幅度约 6‰)且该标准可与 Newark 磁极性序列 E20r(处于 205.7 Ma 位置)相对应。长瑞替期持续时间为~8 Myr, 其底界以牙形石 *Mi. posthermannsteini* sensu lato 首现为标志^[32-34]。在奥地利 Steinbergkogel 剖面, 其磁极性序列 E3r 和诺利—瑞替阶的生物地层标准可与 Newark 盆地磁极性序列 E16r 相对应, 从而得出瑞替

阶底界为 209.5 Ma^[34](即长瑞替期)。Li et al.^[13]在四川盆地须家河剖面进行了旋回地层学和磁性地层学研究, 其能够与 Newark 磁极性序列和意大利 Pignola-Abriola 剖面的磁极性序列相对应^[13,29,31]。基于此, Li et al.^[13]将 NRB 限制在~135 m 处。而根据海相诺利—瑞替期碳同位素波动特征和古生物化石组合^[4], Jin et al.^[2]将 NRB 限制在~129.5 m 处, 并依据 Li et al.^[13]的数据, 计算出研究剖面的沉积时间跨度为~206 Ma 至~205.7 Ma(图2)。

3 样品采集和分析方法

在须家河剖面, 以不超过 2 m 的间隔距离在诺利—瑞替阶采集了 34 件样品, 用于主微量元素测试。首先用锉刀处理样品, 去除表面灰尘和风化部分, 然后用去离子水冲洗, 再将样品放在 50 °C 的烤箱中烘干 8 h, 最后用玛瑙钵研磨成粉至 200 目以下。样品制备在成都理工大学材料与化工学院完成。

34 件样品的主、微量元素分析在中国科学院地

球环境研究所完成。首先将大约0.6克样品粉末与6克干式四硼酸锂($\text{Li}_2\text{B}_4\text{O}_7$)充分混合,在1 000 ℃下熔融5 min,融成玻璃微珠,然后使用X射线荧光光谱仪(WD-XRF; PANalytical, Ea Almelo, The Netherlands)

扫描玻璃微珠,分析精度优于2%。使用了两个国际标准(GSS-8和GSD-12)。样品主量元素、微量元素的测试分析结果分别见表1、2,其中K、Al、Zn、Ni、Rb元素含量引自文献[2]。

表1 须家河组诺利—瑞替阶样品主量元素含量表

Table 1 Major element variations in the bulk rocks of the Norian-Rhaetian transition from the Xujiahe Formation

高度/m	SiO_2	Al_2O_3	Fe_2O_3	MgO	CaO	Na_2O	K_2O	TiO_2	MnO	P_2O_5
105.50	55.17	18.22	6.52	2.50	3.53	0.68	4.17	0.76	0.04	0.14
107.00	56.18	13.07	4.53	3.82	7.08	0.93	2.67	0.69	0.03	0.15
107.40	52.09	12.28	4.79	3.99	9.94	0.90	2.60	0.64	0.04	0.15
109.05	62.91	16.42	6.46	1.90	0.75	0.73	3.24	0.89	0.03	0.15
109.50	80.86	8.14	2.84	0.84	0.35	0.84	1.49	0.63	0.03	0.09
110.20	70.27	13.25	4.40	1.51	0.54	0.80	2.43	0.98	0.03	0.10
111.00	58.29	18.17	6.22	2.51	1.23	0.67	3.53	0.87	0.03	0.14
112.50	56.73	17.58	7.70	2.61	1.80	0.71	3.90	0.81	0.06	0.17
114.50	55.54	14.12	5.30	3.23	6.99	0.93	3.04	0.71	0.06	0.17
115.00	55.98	11.76	4.60	2.39	9.58	0.98	2.42	0.63	0.07	0.15
115.50	61.15	11.28	5.57	1.82	6.89	1.05	2.19	0.64	0.13	0.15
116.50	62.29	10.77	4.06	1.46	8.11	0.97	2.18	0.55	0.05	0.14
117.00	58.39	14.60	5.37	2.44	5.57	0.93	2.99	0.81	0.06	0.15
119.00	53.70	16.35	5.86	2.25	6.61	0.66	3.68	0.62	0.05	0.16
119.50	48.02	11.73	4.72	2.69	14.09	0.85	2.45	0.60	0.10	0.14
120.00	40.12	9.99	3.98	2.72	22.16	0.84	2.10	0.53	0.10	0.14
120.50	37.93	8.59	3.63	3.73	23.03	0.79	1.75	0.45	0.09	0.12
121.00	38.53	9.79	5.03	4.21	19.85	0.73	2.01	0.50	0.08	0.11
121.50	43.31	5.49	2.35	2.29	24.69	0.90	1.13	0.32	0.06	0.09
122.20	48.72	10.62	4.28	2.85	15.10	0.84	2.21	0.54	0.04	0.12
122.50	38.83	9.33	3.60	4.45	20.69	0.78	1.96	0.48	0.05	0.10
123.40	44.59	19.95	3.05	1.32	3.66	0.62	3.14	0.61	0.01	0.05
123.45	57.55	18.99	1.92	1.60	0.86	0.62	3.76	0.66	0.01	0.04
123.75	75.65	12.45	1.67	0.62	0.27	0.98	2.52	0.71	0.01	0.05
123.85	73.41	13.33	2.66	0.95	0.37	1.01	2.73	0.80	0.01	0.09
124.00	70.94	13.75	3.67	1.27	0.53	0.99	2.73	0.77	0.02	0.12
127.00	64.04	7.83	3.14	1.55	8.77	1.07	1.80	0.42	0.05	0.11
128.00	64.10	7.90	3.16	2.31	8.12	1.24	1.82	0.42	0.05	0.11
130.20	66.45	8.12	3.22	1.48	7.35	1.18	1.92	0.42	0.05	0.12
132.50	61.47	7.98	3.18	2.44	8.77	1.20	1.89	0.43	0.05	0.12
133.50	66.06	8.53	3.55	1.25	7.74	1.04	2.00	0.43	0.04	0.12
134.00	62.19	7.74	2.83	2.33	9.11	1.21	1.84	0.40	0.06	0.11
135.00	62.91	7.79	2.85	1.84	10.13	1.14	1.86	0.41	0.06	0.11
137.70	58.45	13.67	4.52	1.84	6.38	0.78	3.16	0.68	0.03	0.15

注:主量元素单位为%;表中K、Al和Zn元素含量引自文献[2]。

表2 須家河組諾利—瑞替階樣品微量元素含量表

Table 2 Trace element variations in the bulk rocks of the Norian-Rhaetian transition from the Xujiahe Formation

高度/m	V	Cr	Ni	Zn	Ga	Rb	Sr	Y	Zr	Nb	Ba	Pb
105.50	144.69	123.79	50.31	108.16	25.31	173.94	100.18	24.73	145.91	20.07	672.38	37.00
107.00	135.56	86.77	45.83	67.37	17.49	115.68	120.94	21.90	204.95	16.28	393.48	27.91
107.40	95.60	87.30	35.29	75.44	15.24	114.18	159.48	25.92	169.63	11.57	401.78	23.12
109.05	160.32	112.47	60.22	85.09	20.49	148.60	74.88	28.97	229.07	18.97	460.21	28.11
109.50	64.98	48.05	21.01	62.96	11.49	61.70	39.62	25.05	310.93	13.22	252.35	—
110.20	103.36	86.45	55.22	59.50	18.88	104.80	63.23	31.04	376.88	21.33	387.70	19.55
111.00	146.37	104.75	47.18	119.17	25.10	177.33	84.51	30.27	182.44	18.60	450.96	34.84
112.50	138.19	109.83	76.49	123.89	21.78	171.55	86.95	28.97	156.52	20.65	577.07	97.96
114.50	124.55	87.93	42.49	91.28	19.53	129.44	120.62	30.60	179.73	18.68	494.26	37.55
115.00	87.74	77.14	41.55	74.81	18.45	101.61	94.15	27.77	187.84	15.43	382.97	21.85
115.50	86.16	79.89	42.28	65.69	16.96	94.13	93.19	23.97	211.36	14.16	464.94	30.56
116.50	72.00	69.95	37.59	73.24	14.28	86.74	79.32	21.57	176.23	11.49	407.98	37.71
117.00	110.92	105.92	49.69	92.74	19.63	126.45	93.72	25.38	207.45	21.01	506.45	40.88
119.00	129.59	92.59	44.79	95.58	21.45	157.58	113.10	25.92	128.90	13.80	603.55	35.78
119.50	113.75	73.02	36.75	76.60	15.35	106.20	182.45	27.23	147.41	15.91	414.50	40.01
120.00	77.88	74.92	49.17	75.13	12.46	93.73	237.19	24.95	128.40	12.62	359.12	37.66
120.50	78.19	62.02	43.74	56.57	12.03	79.76	249.79	19.94	105.98	8.07	293.33	34.72
121.00	99.27	66.67	30.81	64.01	10.96	101.61	241.43	20.60	102.88	11.08	367.94	42.51
121.50	49.14	35.36	18.50	29.30	8.71	46.84	304.75	19.51	153.22	6.40	212.94	18.19
122.20	104.52	70.80	36.65	56.36	13.53	99.12	181.39	18.53	185.34	9.14	328.96	25.22
122.50	90.36	58.84	39.26	56.88	8.17	99.32	275.52	20.70	127.00	9.07	341.36	28.45
123.40	182.45	90.05	22.05	4.77	23.49	231.51	100.92	61.59	179.53	25.24	429.21	104.19
123.45	124.34	92.38	9.32	16.20	27.02	191.00	73.29	18.97	135.60	17.33	470.93	5.27
123.75	62.67	67.62	7.24	10.85	15.24	101.41	53.07	25.92	328.64	15.25	395.37	11.72
123.85	82.39	89.84	24.45	32.13	19.53	113.18	56.98	25.05	261.79	19.12	430.26	15.56
124.00	102.73	85.08	45.52	63.70	15.67	114.38	57.94	31.14	275.30	17.51	434.89	16.20
127.00	70.32	85.61	43.53	31.30	6.99	55.42	108.34	18.53	253.59	10.36	350.61	16.62
128.00	57.95	103.59	33.83	39.89	8.49	63.90	115.32	18.75	227.97	10.64	389.91	14.83
130.20	55.12	90.37	44.99	33.60	9.67	64.50	120.09	18.10	243.08	9.56	404.73	34.21
132.50	56.69	77.14	31.12	32.87	8.92	65.39	120.51	16.46	216.46	8.79	336.21	7.36
133.50	45.15	91.32	33.63	31.61	11.17	70.18	116.07	18.31	235.88	8.51	379.82	14.78
134.00	51.97	73.65	37.69	33.08	8.39	60.01	123.69	16.57	230.57	8.73	320.76	19.09
135.00	57.32	86.45	29.77	29.30	7.21	59.91	132.69	22.23	213.56	9.86	341.25	21.89
137.70	131.47	103.80	52.92	56.15	17.49	133.24	94.99	21.14	253.39	14.41	399.26	22.15

注:微量元素单位为 ug/g; 表中Ni和Rb元素含量引自文献[2]。

4 测试结果与分析

4.1 主微量元素含量

须家河剖面须家河组样品主、微量元素含量见表1、2。其中,诺利末期(剖面:105.5~129.5 m)样品 SiO_2 的含量介于37.93%~80.8%(平均值为56.62%); Al_2O_3 的含量介于5.49%~19.95%(平均值为12.71%); Fe_2O_3 的含量介于1.67%~7.70%(平均值为4.32%); MgO 的含量介于0.62%~4.45%(平均值为2.35%); CaO 的含量介于0.27%~24.69%(平均值为8.26%); Na_2O 的含量介于0.62%~1.24%(平均值为0.86%); K_2O 的含量介于1.13%~4.17%(平均值为2.59%);Rb的含量介于46.84~231.51 $\mu\text{g/g}$ (平均值为116.47 $\mu\text{g/g}$);Sr的含量介于39.62~304.75 $\mu\text{g/g}$ (平均值为127.22 $\mu\text{g/g}$)。

NRB时期(剖面:129.5~135 m)样品 SiO_2 的含量介于61.47%~66.45%(平均值为63.82%); Al_2O_3 的含量介于7.74%~8.53%(平均值为8.03%); Fe_2O_3 的含量介于2.83%~3.55%(平均值为3.13%); MgO 的含量介于1.25%~2.44%(平均值为1.87%); CaO 的含量介于7.35%~10.13%(平均值为8.62%); Na_2O 的含量介于1.04%~1.21%(平均值为1.15%); K_2O 的含量介于1.84%~2.00%(平均值为1.90%);Rb的含量介于59.91~70.18 $\mu\text{g/g}$ (平均值为64.00 $\mu\text{g/g}$);Sr的含量介于116.07~132.69 $\mu\text{g/g}$ (平均值为122.61 $\mu\text{g/g}$)。由于瑞替早期样品数量过少(图2),此阶段的古气候变化在本文不做讨论。

4.2 化学风化指标对古气候的指示

根据风化物质的化学成分,化学风化指标可用来量化风化程度,主要用于示踪古气候记录^[35~38]。本文总结了常见的化学风化指标,并列出了详细的计算公式(表3)^[35~36,39~44]。这些指标涉及不同的元素,因此可以综合对比讨论化学风化对沉积物成分的影响^[45]。例如,钾交代作用对化学蚀变指数(CIA)影响很大,但对化学风化指数(CIW)没有影响^[39];Na消耗指数(τNa)对沉积再旋回和分选导致的石英富集十分灵敏,但这通常不影响CIA值^[45~46]。须家河组NRT时期的四个代表性风化指标:CIA、CIW、斜长石蚀变指数(PIA)、硅铝比指数(R)在地层垂向上的变化趋势如图2所示。

研究表明,高CIA值(80~100)指示炎热潮湿气候条件下强烈的化学风化作用;中等CIA值(70~80)

反映温暖潮湿的气候条件下中等化学风化作用;较低的CIA值(50~70)指示寒冷干燥气候条件下较弱的化学风化作用^[36,47~48]。Ruxton^[35]提出了一种简单的风化指数,Chittleborough^[49]将其称为Ruxton比(R),Ruxton^[35]认为R最适用于均匀酸性到中性母岩的风化剖面,风化过程中 Al_2O_3 含量恒定,并产生高岭土风化产物。R将硅损失量与全元素损失量联系起来,当R大于10时,表明母岩基本没有受到风化作用,R值等于0时,表明母岩受到剧烈的风化作用^[35]。本次研究的样品受到了K交代作用的影响(详情见5.1.1),因此有必要对CIA进行K校正(用CIA_{corr}表示K校正后的CIA)。诺利末期(剖面:105.5~129.5 m),CIA_{corr}(58~81)和R值(3.8~16.9)的平均值分别为73、8.2,表明研究区此时整体上受到了中等强度的化学风化作用,气候条件为温暖湿润气候;在NRB时期(剖面:129.5~135 m),CIA_{corr}(59~64)和R值(13.1~13.9)的平均值分别为61和13.5,表明研究区在该时期受到较弱的化学风化作用,存在降温趋势。

4.3 微量元素对古气候指示

Long *et al.*^[50]提出Rb/Sr值可以用来反映风化作用的程度。大多数岩石的Rb/Sr比值随化学风化程度的增加而增大。这是因为Rb⁺是一种碱性微量元素,相对于选择性浸出的Sr²⁺,它仍然保留在风化后的岩石中^[44,51]。因此,可以利用Rb/Sr比值来评价源区化学风化强度:Rb/Sr>1指示化学风化程度较高;Rb/Sr<1指示化学风化程度中一低^[52]。诺利末期样品(剖面:105.5~129.5 m)的Rb/Sr值介于0.2~2.6,平均值为1.2,表明该时期总体风化程度较高;在NRB时期(剖面:129.5~135.0 m)Rb/Sr比值集中在0.5~0.6,平均值为0.5,指示较低的风化程度。此外,沉积物中Ti元素含量的变化能够反映陆源物质的输入程度,Ti含量越高反映陆源物质越丰富,指示一种温暖湿润的气候条件^[53~54]。图2中可以看出Ti含量变化所指示的气候状况与前文分析的气候变化趋势一致。

样品在剖面的105.5 m、110.7~122.8 m、119.0 m、123.2~124.4 m、137.7 m处CIA和Rb/Sr值相对较高,R值相对较低;在106.6~108.0 m、115.3~116.6 m、121.5 m、126.4~134.5 m处CIA和Rb/Sr值相对较低,R值相对较高(表4)。结合前文分析,认为NRT时期古气候频繁波动,存在温暖潮湿气候和凉爽干燥气候交替出现的现象(图2)。

表3 化学风化指标综合表

Table 3 Summary of chemical weathering indices and their computational formulae

序号	指标名称	表达公式	参考文献
1	硅铝比指数 (R: Ruxton Ratio)	= $\text{SiO}_2/\text{Al}_2\text{O}_3$	Ruxton ^[35]
2	化学蚀变指数 (CIA: Chemical Index of Alteration)	= $\text{Al}_2\text{O}_3/(\text{Al}_2\text{O}_3+\text{Na}_2\text{O}+\text{K}_2\text{O}+\text{CaO}^*) \times 100$	Nesbitt <i>et al.</i> ^[36]
3	化学风化指数 (CIW: Chemical Index of Weathering)	= $\text{Al}_2\text{O}_3/(\text{Al}_2\text{O}_3+\text{Na}_2\text{O}+\text{CaO}^*) \times 100$	Harnois ^[39]
4	斜长石蚀变指数 (PIA: Plagioclase Index of Alteration)	= $(\text{Al}_2\text{O}_3-\text{K}_2\text{O})/(\text{Al}_2\text{O}_3-\text{K}_2\text{O}+\text{Na}_2\text{O}+\text{CaO}^*) \times 100$	Fedo <i>et al.</i> ^[40]
5	Na消耗指数 (τNa: Chemical weathering depletion)	= $(\text{Na/Zr})_{\text{样品}}/(\text{Na/Zr})_{\text{母岩}}$	Rasmussen <i>et al.</i> ^[41]
6	损失化学风化指标 (LCWP: Loss chemical weathering proxy)	= $(\text{CaO}^*+\text{Na}_2\text{O}+\text{MgO})/\text{TiO}_2$	Yang <i>et al.</i> ^[42]
7	成分变异指数 (ICV: Index of compositional variability)	= $(\text{Fe}_2\text{O}_3+\text{K}_2\text{O}+\text{Na}_2\text{O}+\text{CaO}^*+\text{MgO}+\text{MnO}+\text{TiO}_2)/\text{Al}_2\text{O}_3$	Cox <i>et al.</i> ^[43]

注:除τNa和LCWP公式使用质量百分数外,其他公式氧化物参数均使用摩尔为单位。表中CaO^{*}指硅酸盐矿物中的CaO,在无法单独获得硅酸盐矿物中CaO含量时,有必要对CaO含量进行校正。用McLennan *et al.*^[44]提出的方法计算CaO^{*}:CaO剩余=CaO-P₂O₅×10/3,若计算后的CaO_{剩余}<Na₂O,令CaO^{*}=CaO_{剩余};若CaO_{剩余}>Na₂O,令CaO^{*}=Na₂O。

5 讨论

5.1 化学风化指标的适用性分析

本次研究所使用的风化指标有CIA、CIW、PIA、R等(表3)。然而,沉积后成岩蚀变、沉积再旋回以及水动力分选都会对样品的化学成分产生影响^[40,45,55-56]。因此,有必要对化学风化指标的适用性进行评估。

5.1.1 沉积后成岩蚀变对样品的影响

沉积后成岩蚀变会改变沉积物的主要化学成分,从而影响化学风化指标的真实性,因此需要评价其对样品的影响^[57]。如果仅岩石成分是风化的控制因素,样品的风化趋势应平行于A-CN-K图中的A-CN界线^[37,44,52,58]。然而,所研究的样品略微偏向K顶点(图3a^[59]),表明存在K交代作用^[40,58]。富钾孔隙水和黏土矿物在沉积后成岩作用过程中,会使样品富集K₂O,从而导致CIA值偏低^[40]。因此,需要对CIA进行K校正^[57]。本文利用Panahi *et al.*^[60]提出的方法校正CIA:

$$\text{CIA}_{\text{corr}} = \text{Al}_2\text{O}_3/(\text{Al}_2\text{O}_3 + \text{Na}_2\text{O} + \text{K}_2\text{O}^* + \text{CaO}^*) \times 100 \quad (2)$$

$$\text{K}_2\text{O}^* = [\text{m} \times \text{Al}_2\text{O}_3 + \text{m} \times (\text{CaO}^* + \text{Na}_2\text{O})]/(1 - \text{m}) \quad (3)$$

$$\text{m} = \text{K}_2\text{O}/(\text{Al}_2\text{O}_3 + \text{CaO}^* + \text{Na}_2\text{O} + \text{K}_2\text{O}) \quad (4)$$

式中:K₂O^{*}是指发生K交代作用前沉积物中K₂O的含量,m代表母岩中K₂O的比例。前人研究认为晚三叠世四川盆地物源为南秦岭造山带^[61-62],因此母岩中各

元素含量取自南秦岭上地壳岩石中各元素的平均含量^[59]。

因为CIW、PIA指标不受K交代作用的影响^[39-40],因此可以用CIW和PIA值来检验CIA_{corr}值^[57],CIA_{corr}与CIW($r^2=1$)、PIA($r^2=0.9987$)之间都具有很强的相关性(图4a,b),表明K校正消除了K交代作用带来的影响。

5.1.2 沉积再旋回和水动力分选(岩性差异)对样品的影响

再旋回的原岩在被二次风化后,会使CIA值偏大,因此不能准确地指示古气候和源区风化程度^[43,46,55,63]。Cox *et al.*^[43]提出了成分变异指数(ICV),可以用来评估碎屑岩的成分成熟度,从而判断岩石序列是首次沉积的产物还是源于再旋回的沉积物:ICV>1,表明沉积物中含有很少的黏土矿物,属于构造活动背景下的初始沉积^[55,64];ICV<1,则表明沉积物中含有大量的黏土矿物,代表其可能在初始沉积条件下经历了较强烈的风化作用或经历了再旋回沉积作用^[55,65]。从图3b中可以看出大部分样品的ICV>1,表明沉积物整体属于构造活动背景下的初始沉积,受到较弱的沉积再旋回作用的影响。此外,四川盆地三叠统为泥炭沼泽—陆相湖泊—河流沉积序列^[66],下伏地层为元古代—中三叠世海相碳酸盐岩^[19]。因此,下伏地层不太可能为盆地提供再旋回硅质碎屑物质。综上,沉积再旋回作用对四川盆地晚三叠沉积体系影响不大。

**表4 四川盆地须家河组诺利—瑞替之交地球化学数据及
地球化学参数**

**Table 4 Geochemical data and proxies in the bulk
rocks of the Norian-Rhaetian transition from the
Xujiahe Formation, Sichuan Basin**

高度/m	CIA _{corr}	CIW	PIA	ICV	τNa	LCWP	R	Rb/Sr	Ti%
105.50	80	89	86	1.0	0.7	5.0	5.1	1.7	0.5
107.00	73	81	77	1.5	0.7	8.1	7.3	1.0	0.4
107.40	72	80	76	1.6	0.6	8.9	7.2	0.7	0.4
109.05	79	88	85	1.0	0.8	3.6	6.5	2.0	0.5
109.50	73	82	78	1.0	0.8	3.0	16.9	1.6	0.4
110.20	78	87	84	1.0	0.9	2.8	9.0	1.7	0.6
111.00	80	89	87	1.0	0.8	4.4	5.5	2.1	0.5
112.50	79	88	85	1.1	0.7	4.9	5.5	2.0	0.5
114.50	74	82	78	1.3	0.6	7.0	6.7	1.1	0.4
115.00	70	79	74	1.3	0.6	6.7	8.1	1.1	0.4
115.50	69	77	72	1.3	0.7	5.9	9.2	1.0	0.4
116.50	69	77	73	1.2	0.6	6.0	9.8	1.1	0.3
117.00	74	83	79	1.2	0.7	5.2	6.8	1.3	0.5
119.00	79	88	85	1.0	0.7	5.6	5.6	1.4	0.4
119.50	72	81	76	1.4	0.6	7.2	7.0	0.6	0.4
120.00	70	78	74	1.5	0.6	8.2	6.8	0.4	0.3
120.50	69	77	72	2.0	0.5	11.6	7.5	0.3	0.3
121.00	72	80	76	2.0	0.5	11.2	6.7	0.4	0.3
121.50	58	65	59	2.2	0.6	12.5	13.4	0.2	0.2
122.20	71	79	75	1.5	0.7	8.2	7.8	0.5	0.3
122.50	70	78	74	2.0	0.6	12.4	7.1	0.4	0.3
123.40	81	91	89	0.6	0.8	4.1	3.8	2.3	0.4
123.45	81	90	88	0.6	0.7	4.2	5.2	2.6	0.4
123.75	77	86	83	0.7	0.8	2.5	10.3	1.9	0.4
123.85	77	86	83	0.8	0.7	2.8	9.4	2.0	0.5
124.00	77	86	82	0.9	0.8	3.4	8.8	2.0	0.5
127.00	62	69	63	1.5	0.7	8.6	13.9	0.5	0.3
128.00	59	66	59	1.8	0.6	11.1	13.8	0.6	0.3
130.20	61	68	61	1.5	0.7	8.9	13.9	0.5	0.3
132.50	60	67	60	1.9	0.6	11.1	13.1	0.5	0.3
133.50	64	71	65	1.4	0.7	7.4	13.2	0.6	0.3
134.00	59	66	59	1.9	0.6	11.5	13.7	0.5	0.2
135.00	61	68	61	1.7	0.6	9.7	13.7	0.5	0.2
137.70	76	84	80	1.1	0.8	4.9	7.3	1.4	0.4

沉积物在搬运过程中可能受到水动力分选作用,使得黏土矿物及云母类矿物富集于细粒沉积物中,而石英、长石和锆石等矿物富集于粗粒沉积物中^[45-46]。矿物在不同粒级沉积物中富集导致化学元素也呈现类似规律,Si和高场强元素(U、Th、Zr、Hf)趋于富集在石英和重矿物中,大部分主微量元素则趋于富集在细粒沉积物中^[67],从而影响化学风化指数。在相同风化条件下,细粒沉积物比粗粒沉积物

具有更高的CIA值^[68]。Al/Si比值可作为碎屑岩粒度(岩性)和水动力分选的指标^[69-70],此次样品其变化范围为0.1~0.5。损失化学风化指数(LCWP)和τNa是基于分选敏感元素Zr和Ti计算的风化指数^[45],与Al/Si存在弱相关性(图3c,d)。因此,在研究区沉积物的形成过程中,岩性差异对样品的影响较弱。

综上,分析了沉积后成岩蚀变、沉积再旋回以及水动力分选对样品的影响后,表明本文的实验数据可用于反映物源区的化学风化程度和古气候。此外,大多数风化指标(CIW、PIA、R、LCWP)与CIA_{corr}都具有良好的相关性(图4),指示这些指标均适用于指示须家河组沉积岩的源区化学风化强度^[71]。

5.2 NRB时期全球降温事件

本文系统地研究了须家河组NRT时期的主、微量元素,并运用元素地球化学指标重建了特提斯东缘四川盆地广元地区须家河组NRT时期的古气候,即在诺利末期CIA_{corr}、Rb/Sr相对较高,R值相对较低(平均值分别为73.0、1.2、8.2),而NRB时期CIA_{corr}、Rb/Sr相对较低,R值相对较高(平均值分别为61.0、0.5、13.5),揭示了诺利末期温暖潮湿的气候条件和NRB存在的一次降温事件(详情见3.2、3.3)。本次降温事件可能是全球性的,且能够被同位素地球化学(牙形石δ¹⁸O)、古植物学及沉积学的证据所支持^[3,5,16,72-73]。

5.2.1 同位素地球化学证据

Trotter et al.^[5]利用牙形石的氧同位素数据定量化分析诺利—瑞替期的古海水温度,从而判别当时西特提斯地区该时期的古气候状况。其在意大利Lagonegro盆地的中—上诺利阶(Alaunian-Sevatician)界线附近发现了牙形石氧同位素的一次大幅度负偏,估计当时的表层海水温度上升了大约7℃(变暖事件W3),而后温度逐渐缓慢下降直到诺利阶和瑞替阶界线的附近,反映了短暂的降温事件(图5)^[2,4-5,13,29,34,74-77]。同样,来自加拿大Cordillera地区的牙形石氧同位素数据显示中—上诺利阶界线附近表层海水温度可达35℃,支持了诺利中—晚期气候条件较热的观点^[78]。

5.2.2 古植物学证据

中生代大多数蕨类植物生长在沼泽、河岸、林下等温暖潮湿的气候环境下^[79],而大多数苏铁类植物能够适应干旱的气候条件^[80]。此外,银杏树和针叶树都属于落叶乔木,通常分布于相对干燥的温带

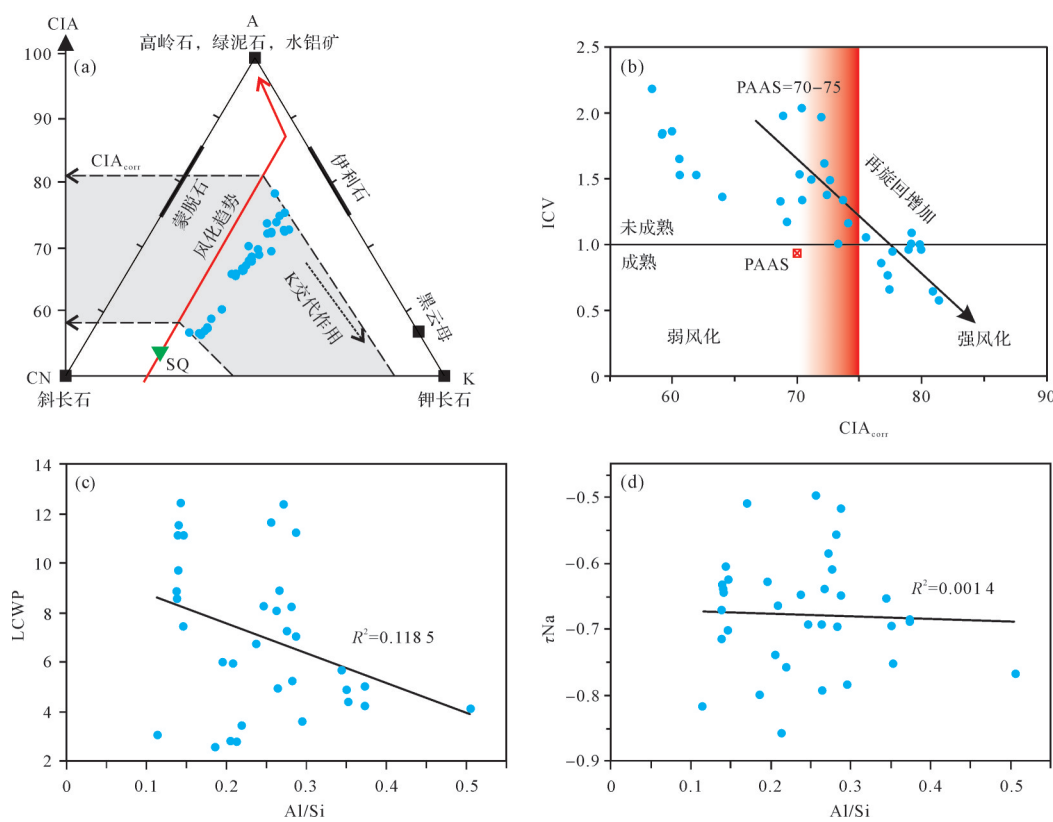


图3 (a) A-CN-K图; (b) ICV-CIA图解; (c) Al/Si与损失化学风化指数(LCWP)的相关性图;
(d) Al/Si与 τ_{Na} 的相关性图

图a显示了南秦岭上地壳(SQ)的风化趋势^[59],以供比较,A-Al₂O₃,CN-CaO⁺+Na₂O,K-K₂O;图b中ICV为成分变异指数

Fig.3 (a) Plots of A-CN-K; (b) diagram of ICV-CIA; (c) correlations between Al/Si and loss chemical weathering proxy (LCWP); (d) correlations between Al/Si and τ_{Na}

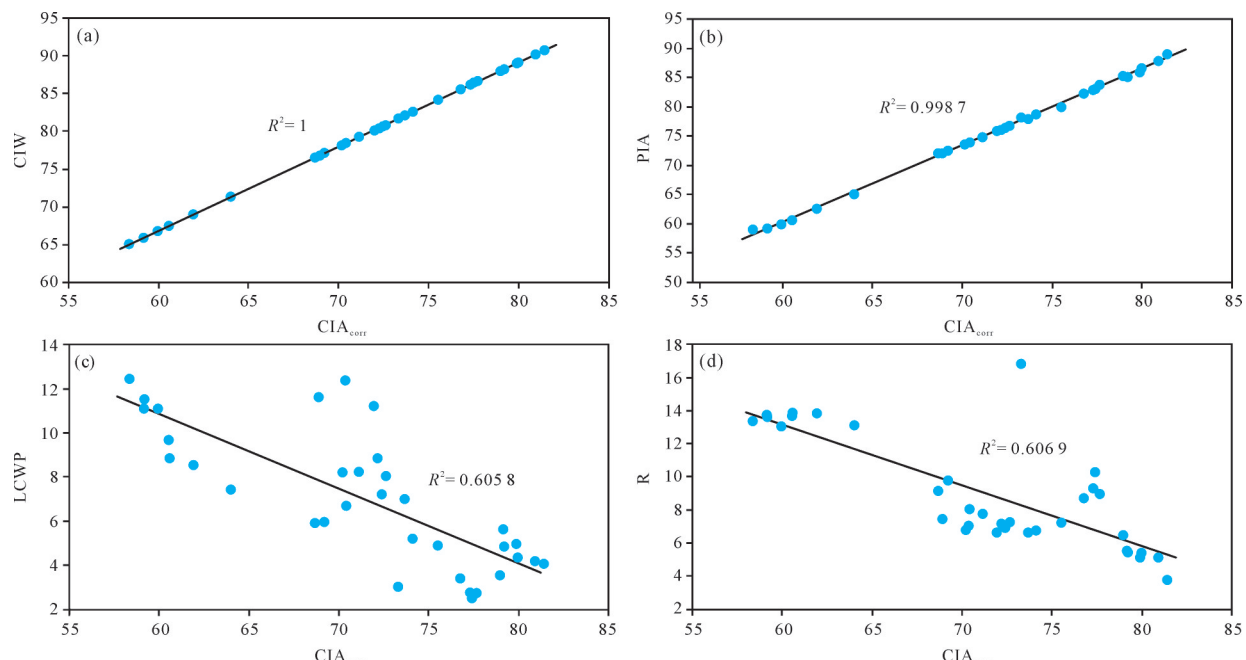


图4 K校正后的化学蚀变指数与其他风化指数的相关性图

Fig.4 Correlations between the K-corrected chemical index of alteration and other weathering indices

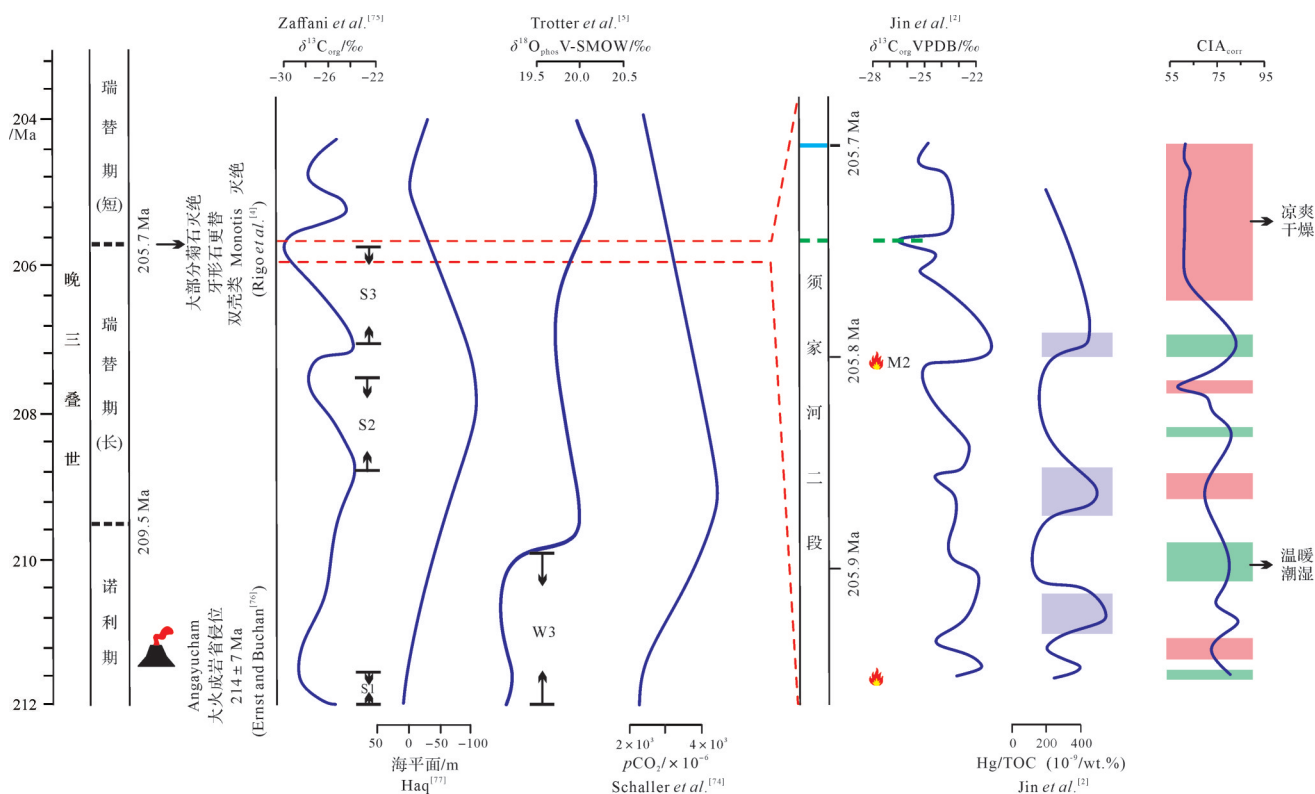


图5 诺利—瑞替期之交的地质事件和地球化学曲线综合图

短瑞替期底界(205.7 Ma)为Li et al.^[13]和Maron et al.^[29]根据磁性地层学、碳同位素以及牙形石所限制;长瑞替期底界(209.5 Ma)为Hüsing et al.^[34]根据磁性地层学和牙形石所限制;绿色虚线为Jin et al.^[2]和Rigo et al.^[4]根据碳同位素限制的瑞替期底界;须家河二段时间尺度、野火信息、 $\delta^{13}\text{C}_{\text{org}}$ VPDB/Hg/TOC据Jin et al.^[2],其中淡蓝色方块为Hg浓度异常层位;生物绝灭据Rigo et al.^[4]; $\delta^{18}\text{O}_{\text{phos}}$ V-SMOW 和W3据Trotter et al.^[5],其中W3为变暖事件; $p\text{CO}_2$ 变化趋势据Schaller et al.^[74]; $\delta^{13}\text{C}_{\text{org}}$ 变化趋势及S1、S2和S3据Zaffani et al.^[75],其中,S1、S2和S3为碳同位素负漂;Angayucham大火成岩省侵位时间据Ernst et al.^[76];海平面升降据Haq^[77]

Fig.5 Geological events and geochemical curves across the Norian-Rhaetian transition

地区,具有较强的抗寒能力^[3]。Li et al.^[15]在四川盆地合川地区须家河组进行了孢粉学研究,发现晚三叠世植被经历了由低地蕨类林向乔木较多的混合林的变化(蕨类逐渐被银杏、针叶植物及苏铁类植物取代),反映了晚三叠世早期的气候条件相对温暖湿润,而诺利末期至瑞替期总体呈降温干燥趋势。此外,Lu et al.^[3]在川东北七里峡剖面上三叠统须家河组一段中发现的植物化石以 *Dictyophyllum*、*Clathropteris* 及 *Cladophlebis* 等蕨类植物为主,到了须家河组二段蕨类植物则被已适应干旱环境的 *Neocalamites* 所取代,成为该时期植物群落的优势种,Lu et al.^[3]认为晚三叠世的古气候总体为温暖湿润,但在NRB时期出现了短暂的凉爽干燥的气候环境。在古植物的研究中,化石木 *Xenoxyylon* 的出现是凉爽气候条件的标志^[14,81-82],川西北须家河组二段中化石木 *Xenoxyylon*(图2)的发现也佐证了NRB时期凉爽的气候特征^[14]。同样,Li et al.^[16]对四川盆地宣汉地区须家河组(诺利—瑞替阶)进行了详细的孢

粉研究,发现诺利晚期至NRB时期蕨类占比从~50%急剧下降到~30%,而针叶树和苏铁/银杏类占比分别上升了~15%和~10%,揭示NRB时期存在降温事件。

5.2.3 沉积学证据

Berra et al.^[72-73]发现特提斯西缘阿尔卑斯山脉中部的上三叠统沉积序列在NRB附近突然从碳酸盐沉积向细粒硅质碎屑沉积转变,且伴随着早期白云石化作用的终止,Berra et al.^[72-73]将其归因于全球降温导致的海平面迅速下降,如图5所示^[77](以长瑞替期为时间轴)。此外,Lu et al.^[3]在特提斯东缘四川盆地七里峡剖面须家河组(诺利—瑞替阶)进行了沉积特征分析,认为须一段主要为泥岩和页岩(占94.4%),属于温暖气候条件下的潟湖相和泥炭沼泽相,而上覆须二段底层为中—细粒的长石砂岩,可能为凉爽干燥气候背景下的河口湾相。因此基于沉积学证据,Lu et al.^[3]推测NRB时期存在短暂的降温事件。

5.3 NRT时期的古气候驱动机制探讨

5.3.1 超级季风

本次运用化学风化指标(如:CIA_{corr}、CIW、PIA、R、Rb/Sr、Ti等)揭示了四川盆地须家河组NRT时期的古气候演化特征。在此期间风化指标数值呈高、低交替出现,反映气候波动频繁,存在温暖潮湿气候和凉爽干燥气候交替出现的现象(图2,5),其可能与晚三叠世盛行于泛大陆上的超级季风有关。Olsen *et al.*^[83]分析了Newark超群6 700 m(持续时间~33 Ma)的岩心,揭示了季风的各种周期性变化。最小有0.2~0.3 mm的微层理,呈现暗色和浅色互层,是季风气候的年纹层,其中较大的沉积韵律可相当于季风两万年的岁差周期^[83]。本次研究剖面时间尺度为~0.3 Ma,这种较短时间尺度内的干湿交替,季风可能呈现相当于万年的岁差周期。晚三叠世泛大陆聚合,古气候带呈带状分布^[84],季风环流增强^[85-89],导致气候波动频繁^[90-91]。同时,四川盆地晚三叠世的风暴沉积^[87]、植物化石^[3]和树木年轮^[92]的研究结果也一致表明,我国中纬度地区晚三叠世为季风性气候,且为受季风驱动的高能量海—陆相环境。此外,西特提斯地区意大利^[73]、匈牙利^[93]、瑞典^[94]以及南半球澳大利亚^[95]的古气候研究,表明晚三叠世巨型季风达到顶峰,且控制了整个泛大陆和特提斯沿岸的气候循环。季风性气候容易形成干—湿交替的循环气候^[88,92],在季风增强的过程中会带来特提斯洋和泛大洋的丰富水分,导致泛大陆和特提斯沿岸气候湿润,反之季风减弱则会导致气候较为干旱^[57]。因此,本文认为晚三叠世的超级季风可能对NRT时期全球气候波动产生了重要的影响^[96-97],且可能导致了NRB时期的降温事件。

5.3.2 火山活动

研究表明,火山活动亦是全球气候变化的主要驱动力之一,大规模火山喷发会释放出大量的温室气体,造成气候变暖^[98]。例如,二叠纪—三叠纪界线事件时期全球增温事件就归因于西伯利亚大火山岩省爆发释放的大量温室气体^[99-100]。Schaller *et al.*^[74]根据北美Newark裂谷盆地成土碳酸盐同位素与古土壤中有机质的碳同位素,发现CO₂浓度从中诺利期的~2 000×10⁻⁶上升到晚诺利期的~4 000×10⁻⁶(图5)。同时,在诺利末期,泛大洋深海盆地中的硅质岩和泥岩序列所记录的¹⁸⁷Os/¹⁸⁸Os值急剧下降^[1,101-102]。此外,Trotter *et al.*^[5]和Sun *et al.*^[78]的牙形石氧同位素数据显

示,在中—上诺利阶(Alaunian-Sevatician)界线附近表层海水温度可达35 °C,与古新世—始新世极热事件记录的相同纬度地区的温度相当^[78]。再者,一些主要的海洋生物群体,例如菊石,牙形石,双壳等在中—晚诺利期开始衰落,并逐渐开始灭绝^[5](图5)。同时,Sun *et al.*^[78]还报道了Alaunian时期珊瑚和海绵的低生物多样性。种种迹象表明诺利—瑞替期地球环境发生了显著的变化,可能与同时期Angayucham大火成岩省的侵位有关^[2,4,75-76,103](图5)。然而Angayucham大火成岩省爆发时间被粗略定在214±7 Ma^[76],与研究剖面(~205.7至~206 Ma)存在一定的时间差距,但关于Angayucham大火成岩省的认识非常有限,不排除其延长至NRB附近。再者,Jin *et al.*^[2]在须家河剖面中发现了至少三套汞元素的富集层位,且伴随着多次有机碳同位素负漂(图2,5),认为该时期可能存在多期次大规模的火山活动^[2]。基于此认识,我们不排除火山活动对四川盆地NRT时期的古气候系统产生了一定影响的可能性,但火山活动的具体时限、量级及其如何与古气候变化相耦合,这些问题仍不清晰,未来需要进一步研究。

5.3.3 野火事件

野火的发生受控于诸多因素,如气候干湿程度、大气氧含量和植被,同时大规模的野火事件也会反过来影响区域或甚至是全球的气候^[104]。在晚三叠世,四川盆地多个地区均有野火事件的记录。在宣汉地区,上三叠统须家河组有较为零星的木炭化石(丝炭)产出,表明野火有一定的复燃时间,可能存在某些氧气水平较低的时期或对气候周期性变化(即较潮湿的时期)的响应^[87]。此外,Song *et al.*^[89]在广元和合川的两个陆相须家河组剖面也发现了以多环芳烃形式存在的野火生物标志物证据,该野火的可能成因是晚三叠世古热带辐合区的南移导致的区域气候干旱化^[89]。在本次研究剖面M2煤层(图2,5)中也记录了一次野火事件,据黑碳含量变化特征,Jin *et al.*^[2]推测此次野火类型为阴燃火,形成于湿润气候的背景。晚三叠世的野火事件不仅在四川盆地存在记录,在全球其他地区也存在相关记录。Ziegler *et al.*^[105]以及Tanner *et al.*^[106]在美国新墨西哥州北部上三叠统Chinle组发现了木炭化石并认为其与古野火相关。美国犹他州东南部上三叠统Chinle组产出的树干化石上存在火痕^[107]且地层中存在丰度很高的丝炭^[106],表明该地区曾发生过野火事件。德国西南部的上三

叠统砂岩中也有木炭化石产出,同样指示古野火事件的存在^[108]。此外,瑞典上三叠统Höganäs组^[109]以及来自波兰Kamień Pomorski剖面和Lipie Śląskie剖面地层^[110]的报道,均表明同时期的地层中有丝炭记录。虽然晚三叠世的野火频发,但目前我们对野火事件仍缺乏精细的时间限定和全球统一比对;此外,晚三叠世野火事件能否驱动同期全球的古气候变化仍不清楚。因此,我们不排除晚三叠世野火事件可能对同期古气候变化产生一定的影响,但其与气候环境的互馈机制仍有待进一步研究。

6 结论

(1) 四川盆地须家河组诺利末期(剖面:105.5~129.5 m)整体上受到中等强度的化学风化作用,气候环境以温暖湿润为主;诺利—瑞替期界线(剖面:129.5~135 m)受到较弱的化学风化作用,存在短暂的降温事件。

(2) 晚三叠世盛行于泛大陆上的超级季风的变化是导致四川盆地须家河组NRT时期气候频繁波动和NRB降温事件的主要原因,且同时期的火山活动和野火事件也对气候变化产生一定的影响,但火山活动和野火事件发生的准确时限以及其如何驱动同时期的气候变化,还需要进一步研究。

致谢 感谢中国科学院地球环境研究所张飞老师和吴枫老师在主微量测试中提供的帮助;感谢三位审稿专家提出的建设性意见和建议,以及编辑部老师的认真校对,使文章质量得到显著提升。

参考文献(References)

- [1] Sato H, Ishikawa A, Onoue T, et al. Sedimentary record of Upper Triassic impact in the Lagonegro Basin, southern Italy: Insights from highly siderophile elements and Re-Os isotope stratigraphy across the Norian/Rhaetian boundary[J]. *Chemical Geology*, 2021, 586: 120506.
- [2] Jin X, Ogg J G, Lu S, et al. Terrestrial record of carbon-isotope shifts across the Norian/Rhaetian boundary: A high-resolution study from northwestern Sichuan Basin, South China[J]. *Global and Planetary Change*, 2022, 210: 103754.
- [3] Lu N, Wang Y D, Popa M E, et al. Sedimentological and paleoecological aspects of the Norian-Rhaetian transition (Late Triassic) in the Xuanhan area of the Sichuan Basin, southwest China [J]. *Palaeoworld*, 2019, 28(3): 334-345.
- [4] Rigo M, Onoue T, Tanner L H, et al. The Late Triassic Extinction at the Norian/Rhaetian boundary: Biotic evidence and geochemical signature[J]. *Earth-Science Reviews*, 2020, 204: 103180.
- [5] Trotter J A, Williams I S, Nicora A, et al. Long-term cycles of Triassic climate change: A new $\delta^{18}\text{O}$ record from conodont apatite [J]. *Earth and Planetary Science Letters*, 2015, 415: 165-174.
- [6] Casacci M, Bertinelli A, Algeo T J, et al. Carbonate-to-biosilica transition at the Norian-Rhaetian boundary controlled by rift-related subsidence in the western Tethyan Lagonegro Basin (southern Italy)[J]. *Palaeogeography, Palaeoclimatology, Palaeoecology*, 2016, 456: 21-36.
- [7] Tanner L H, Hubert J F, Coffey B P, et al. Stability of atmospheric CO_2 levels across the Triassic/Jurassic boundary[J]. *Nature*, 2001, 411(6838): 675-677.
- [8] Schaller M F, Wright J D, Kent D V, et al. Rapid emplacement of the central Atlantic magmatic province as a net sink for CO_2 [J]. *Earth and Planetary Science Letters*, 2012, 323-324: 27-39.
- [9] Williford K H, Grice K, Holman A, et al. An organic record of terrestrial ecosystem collapse and recovery at the Triassic-Jurassic boundary in East Greenland[J]. *Geochimica et Cosmochimica Acta*, 2014, 127: 251-263.
- [10] Steinthorsdottir M, Tosolini A M P, McElwain J C. Evidence for insect and annelid activity across the Triassic-Jurassic transition of East Greenland[J]. *Palaios*, 2015, 30(8): 597-607.
- [11] Dal Corso J, Mills B J W, Chu D L, et al. Permo-Triassic boundary carbon and mercury cycling linked to terrestrial ecosystem collapse[J]. *Nature Communications*, 2020, 11(1): 2962.
- [12] Chen S F, Wilson C J L, Worley B A. Tectonic transition from the Songpan-Garzê fold belt to the Sichuan Basin, south-western China[J]. *Basin Research*, 1995, 7(3): 235-253.
- [13] Li M S, Zhang Y, Huang C J, et al. Astronomical tuning and magnetostratigraphy of the Upper Triassic Xujiahe Formation of South China and Newark Supergroup of North America: Implications for the Late Triassic time scale[J]. *Earth and Planetary Science Letters*, 2017, 475: 207-223.
- [14] Tian N, Wang Y D, Philippe M, et al. New record of fossil wood *Xenoxylo* from the Late Triassic in the Sichuan Basin, southern China and its paleoclimatic implications[J]. *Palaeogeography, Palaeoclimatology, Palaeoecology*, 2016, 464: 65-75.
- [15] Li L Q, Wang Y D, Vajda V, et al. Late Triassic ecosystem variations inferred by palynological records from Hechuan, southern Sichuan Basin, China[J]. *Geological Magazine*, 2018, 155(8): 1793-1810.
- [16] Li L Q, Wang Y D, Kürschner W M, et al. Palaeovegetation and palaeoclimate changes across the Triassic-Jurassic transition in the Sichuan Basin, China[J]. *Palaeogeography, Palaeoclimatology, Palaeoecology*, 2020, 556: 109891.
- [17] Yong Y, Allen P A, Densmore A L, et al. Evolution of the Longmen Shan Foreland Basin (western Sichuan, China) during the Late Triassic Indosinian orogeny[J]. *Basin Research*, 2003, 15(1): 117-138.
- [18] 王永栋,付碧宏,谢小平,等. 四川盆地陆相三叠系与侏罗系

- [M]. 合肥:中国科学技术出版社,2010. [Wang Yongdong, Fu Bihong, Xie Xiaoping, et al. The terrestrial Triassic and Jurassic systems in the Sichuan Basin, China[M]. Hefei: University of Science and Technology of China Press, 2010.]]
- [19] Li Y, Yan Z K, Liu S G, et al. Migration of the carbonate ramp and sponge buildup driven by the orogenic wedge advance in the early stage (Carnian) of the Longmen Shan Foreland Basin, China[J]. Tectonophysics, 2014, 619-620: 179-193.
- [20] 李智武,刘树根,陈洪德,等. 龙门山冲断带分段—分带性构造格局及其差异变形特征[J]. 成都理工大学学报(自然科学版), 2008, 35 (4) : 440-454. [Li Zhiwu, Liu Shugen, Chen Hongde, et al. Structural segmentation and zonation and differential deformation across and along the Lomgmen thrust belt, west Sichuan, China[J]. Journal of Chengdu University of Technology (Science & Technology Edition), 2008, 35(4): 440-454.]
- [21] 梅冥相. 中上扬子印支运动的地层学效应及晚三叠世沉积盆地格局[J]. 地学前缘, 2010, 17(4): 99-111. [Mei Mingxiang. Stratigraphic impact of the Indo-China Movement and its related evolution of sedimentary-basin pattern of the Late Triassic in the Middle-Upper Yangtze region, South China[J]. Earth Science Frontiers, 2010, 17(4): 99-111.]
- [22] Scotese C R. Atlas of Permo-Triassic paleogeographic maps (Mollweide Projection), maps 43-52, volumes 3 & 4 of the paleo-map atlas for ArcGIS[M]. Evanston: Paleomap Project, 2014.
- [23] 向芳,肖倩,喻显涛,等. 四川盆地元坝地区上二叠统海相凝灰沉积储层特征[J]. 石油与天然气地质, 2022, 43(4) : 889-901. [Xiang Fang, Xiao Qian, Yu Xiantao, et al. Reservoir characteristics of the Upper Permian marine tuffaceous deposits in Yuanba area, Sichuan Basin[J]. Oil & Gas Geology, 2022, 43 (4): 889-901.]
- [24] Deng T, Li Y, Wang Z J, et al. Geochemical characteristics and organic matter enrichment mechanism of black shale in the Upper Triassic Xujiahe Formation in the Sichuan Basin: Implications for paleoweathering, provenance and tectonic setting[J]. Marine and Petroleum Geology, 2019, 109: 698-716.
- [25] 高彩霞,邵龙义,李长林,等. 四川盆地东部上三叠统须家河组层序地层及聚煤特征研究[J]. 古地理学报, 2009, 11(6) : 689-696. [Gao Caixia, Shao Longyi, Li Changlin, et al. Sequence stratigraphy and coal accumulation of the Upper Triassic Xujiahe Formation in eastern Sichuan Basin[J]. Journal of Palaeogeography, 2009, 11(6): 689-696.]
- [26] 姜在兴,田继军,陈桂菊,等. 川西前陆盆地上三叠统沉积特征[J]. 古地理学报, 2007, 9(2) : 143-154. [Jiang Zaixing, Tian Jijun, Chen Guiju, et al. Sedimentary characteristics of the Upper Triassic in western Sichuan Foreland Basin[J]. Journal of Palaeogeography, 2007, 9(2): 143-154.]
- [27] 郑建屏,秦镜蓉,冯建川. 四川盆地晚三叠世煤炭资源地球物理远景调查[M]. 北京:地质出版社, 1992. [Zheng Jianping, Qin Jingrong, Feng Jianchuan. Geophysical prospecting of Late Triassic coal resources in Sichuan Basin[M]. Beijing: Geological Publishing House, 1992.]
- [28] 夏宗实,袁昌明,李汝宁. 四川盆地陆相中生代地层古生物[M]. 成都:四川人民出版社, 1982. [Xia Zhongshi, Yuan Changming, Li Lunling. Paleontology of continental Mesozoic strata in Sichuan Basin[M]. Chengdu: Sichuan People's Publishing House, 1982.]
- [29] Maron M, Rigo M, Bertinelli A, et al. Magnetostratigraphy, biostratigraphy, and chemostratigraphy of the Pignola-Abriola section: New constraints for the Norian-Rhaetian boundary[J]. GSA Bulletin, 2015, 127(7/8): 962-974.
- [30] Bertinelli A, Casacci M, Concheri G, et al. The Norian/Rhaetian boundary interval at Pignola-Abriola section (southern Apennines, Italy) as a GSSP candidate for the Rhaetian Stage: An update[J]. Albertiana, 2016, 43: 5-18.
- [31] Rigo M, Bertinelli A, Concheri G, et al. The Pignola-Abriola section (southern Apennines, Italy): A new GSSP candidate for the base of the Rhaetian Stage[J]. Lethaia, 2016, 49(3): 287-306.
- [32] Kent D V, Olsen P E, Muttoni G. Astrochronostigraphic polarity time scale (APTS) for the Late Triassic and Early Jurassic from continental sediments and correlation with standard marine stages[J]. Earth-Science Reviews, 2017, 166: 153-180.
- [33] Muttoni G, Kent D V, Jadoul F, et al. Rhaetian magneto-biostratigraphy from the southern Alps (Italy): Constraints on Triassic chronology[J]. Palaeogeography, Palaeoclimatology, Palaeoecology, 2010, 285(1/2): 1-16.
- [34] Hüsing S K, Deenen M H L, Koopmans J G, et al. Magnetostratigraphic dating of the proposed Rhaetian GSSP at Steinbergkogel (Upper Triassic, Austria): Implications for the Late Triassic time scale[J]. Earth and Planetary Science Letters, 2011, 302(1/2): 203-216.
- [35] Ruxton B P. Measures of the degree of chemical weathering of rocks[J]. The Journal of Geology, 1968, 76(5): 518-527.
- [36] Nesbitt H W, Young G M. Early Proterozoic climates and plate motions inferred from major element chemistry of lutites[J]. Nature, 1982, 299(5885): 715-717.
- [37] Nesbitt H W, Young G M. Prediction of some weathering trends of plutonic and volcanic rocks based on thermodynamic and kinetic considerations[J]. Geochimica et Cosmochimica Acta, 1984, 48(7): 1523-1534.
- [38] Price J R, Velbel M A. Chemical weathering indices applied to weathering profiles developed on heterogeneous felsic metamorphic parent rocks[J]. Chemical Geology, 2003, 202(3/4): 397-416.
- [39] Harnois L. The CIW index: A new chemical index of weathering [J]. Sedimentary Geology, 1988, 55(3/4): 319-322.
- [40] Fedo C M, Nesbitt H W, Young G M. Unraveling the effects of potassium metasomatism in sedimentary rocks and paleosols, with implications for paleoweathering conditions and provenance [J]. Geology, 1995, 23(10): 921-924.

- [41] Rasmussen C, Brantley S, Richter D D, et al. Strong climate and tectonic control on plagioclase weathering in granitic terrain[J]. *Earth and Planetary Science Letters*, 2011, 301(3/4): 521-530.
- [42] Yang S L, Ding F, Ding Z L. Pleistocene chemical weathering history of Asian arid and semi-arid regions recorded in loess deposits of China and Tajikistan[J]. *Geochimica et Cosmochimica Acta*, 2006, 70(7): 1695-1709.
- [43] Cox R, Lowe D R, Cullers R L. The influence of sediment recycling and basement composition on evolution of mudrock chemistry in the southwestern United States[J]. *Geochimica et Cosmochimica Acta*, 1995, 59(14): 2919-2940.
- [44] McLennan S M, Hemming S, McDaniel D K, et al. Geochemical approaches to sedimentation, provenance, and tectonics[M]// Johnsson M J, Basu A. Processes controlling the composition of clastic sediments. Geological Society of America, 1993: 21-40.
- [45] Yang J H, Cawood P A, Du Y S, et al. Reconstructing Early Permian tropical climates from chemical weathering indices[J]. *GSA Bulletin*, 2016, 128(5/6): 739-751.
- [46] Garzanti E, Padoan M, Setti M, et al. Weathering geochemistry and Sr-Nd fingerprints of equatorial Upper Nile and Congo muds [J]. *Geochemistry, Geophysics, Geosystems*, 2013, 14(2): 292-316.
- [47] Young G M. Stratigraphic and tectonic settings of Proterozoic glaciogenic rocks and banded iron-formations: Relevance to the snowball Earth debate[J]. *Journal of African Earth Sciences*, 2002, 35(4): 451-466.
- [48] Yan D T, Chen D Z, Wang Q C, et al. Large-scale climatic fluctuations in the Latest Ordovician on the Yangtze Block, South China[J]. *Geology*, 2010, 38(7): 599-602.
- [49] Chittleborough D J. Indices of weathering for soils and palaeosols formed on silicate rocks[J]. *Australian Journal of Earth Sciences*, 1991, 38(1): 115-120.
- [50] Long X P, Sun M, Yuan C, et al. Early Paleozoic sedimentary record of the Chinese Altai: Implications for its tectonic evolution [J]. *Sedimentary Geology*, 2008, 208(3/4): 88-100.
- [51] Nesbitt H W, Markovics G, Price R C. Chemical processes affecting alkalis and alkaline earths during continental weathering [J]. *Geochimica et Cosmochimica Acta*, 1980, 44(11): 1659-1666.
- [52] Asiedu D K, Agoe M, Amponsah P O, et al. Geochemical constraints on provenance and source area weathering of metasedimentary rocks from the Paleoproterozoic (~2.1 Ga) Wa-Lawra Belt, southeastern margin of the West African Craton[J]. *Geodinamica Acta*, 2019, 31(1): 27-39.
- [53] 袁宝印, 陈克造, Bowler J M, 等. 青海湖的形成与演化趋势 [J]. 第四纪研究, 1990, 10(3): 233-243. [Yuan Baoyin, Chen Kezao, Bowler J M, et al. The formation and evolution of the Qinghai Lake[J]. *Quaternary Sciences*, 1990, 10(3): 233-243.]
- [54] 马宝林, 王琪. 青海湖现代沉积物的元素分布特征[J]. 沉积学报, 1997, 15(3): 120-125. [Ma Baolin, Wang Qi, Distribution characteristics of elements in modern sediments of Qinghai Lake [J]. *Acta Sedimentologica Sinica*, 1997, 15(3): 120-125.]
- [55] 徐小涛, 邵龙义. 利用泥质岩化学蚀变指数分析物源区风化程度时的限制因素[J]. 吉地理学报, 2018, 20(3): 515-522. [Xu Xiaotao, Shao Longyi. Limiting factors in utilization of chemical index of alteration of mudstones to quantify the degree of weathering in provenance[J]. *Journal of Palaeogeography*, 2018, 20(3): 515-522.]
- [56] Sun S, Chen A Q, Hou M C, et al. Rapid climatic fluctuations during the Guadalupian-Lopingian transition: Implications from weathering indices recorded in acid-insoluble residues of carbonate rocks, South China[J]. *Journal of Asian Earth Sciences*, 2022, 230: 105222.
- [57] Dai X D, Du Y S, Ziegler M, et al. Middle Triassic to Late Jurassic climate change on the northern margin of the South China Plate: Insights from chemical weathering indices and clay mineralogy[J]. *Palaeogeography, Palaeoclimatology, Palaeoecology*, 2022, 585: 110744.
- [58] Fedo C M, Eriksson K A, Krogstad E J. Geochemistry of shales from the Archean (~3.0 Ga) Buhwa Greenstone Belt, Zimbabwe: Implications for provenance and source-area weathering [J]. *Geochimica et Cosmochimica Acta*, 1996, 60(10): 1751-1763.
- [59] Gao S, Luo T C, Zhang B R, et al. Chemical composition of the continental crust as revealed by studies in East China[J]. *Geochimica et Cosmochimica Acta*, 1998, 62(11): 1959-1975.
- [60] Panahi A, Young G M, Rainbird R H. Behavior of major and trace elements (including REE) during Paleoproterozoic pedogenesis and diagenetic alteration of an Archean granite near Ville Marie, Québec, Canada[J]. *Geochimica et Cosmochimica Acta*, 2000, 64(13): 2199-2220.
- [61] Luo L, Qi J F, Zhang M Z, et al. Detrital zircon U-Pb ages of Late Triassic-Late Jurassic deposits in the western and northern Sichuan Basin margin: Constraints on the foreland basin provenance and tectonic implications[J]. *International Journal of Earth Sciences*, 2014, 103(6): 1553-1568.
- [62] Shao T B, Cheng N F, Song M S. Provenance and tectonic-paleogeographic evolution: Constraints from detrital zircon U-Pb ages of Late Triassic-Early Jurassic deposits in the northern Sichuan Basin, central China[J]. *Journal of Asian Earth Sciences*, 2016, 127: 12-31.
- [63] Gaillardet J, Dupré B, Allègre C J. Geochemistry of large river suspended sediments: Silicate weathering or recycling tracer? [J]. *Geochimica et Cosmochimica Acta*, 1999, 63(23/24): 4037-4051.
- [64] van de Kamp P C, Leake B E. Petrography and geochemistry of feldspathic and mafic sediments of the northeastern Pacific margin[J]. *Transactions of the Royal Society of Edinburgh: Earth Sciences*, 1985, 76(4): 411-449.
- [65] Barshad I. The effect of a variation in precipitation on the nature

- of clay mineral formation in soils from acid and basic igneous rocks[J]. Proceedings International Clay Conference, 1966: 167-173.
- [66] 王鸿祯. 中国古地理图集[M]. 北京: 地图出版社, 1985. [Wang Hongzhen. Atlas of the palaeogeography of China[M]. Beijing: Map Publishing House, 1985.]
- [67] Pang H L, Pan B T, Garzanti E, et al. Mineralogy and geochemistry of modern Yellow River sediments: Implications for weathering and provenance[J]. Chemical Geology, 2018, 488: 76-86.
- [68] Jian X, Guan P, Zhang W, et al. Geochemistry of Mesozoic and Cenozoic sediments in the northern Qaidam Basin, northeastern Tibetan Plateau: Implications for provenance and weathering[J]. Chemical Geology, 2013, 360-361: 74-88.
- [69] Bouchez J, Gaillardet J, France-Lanord C, et al. Grain size control of river suspended sediment geochemistry: Clues from Amazon River depth profiles[J]. Geochemistry, Geophysics, Geosystems, 2011, 12(3): Q03008.
- [70] Lupker M, France-Lanord C, Galy V, et al. Increasing chemical weathering in the Himalayan system since the Last Glacial Maximum[J]. Earth and Planetary Science Letters, 2013, 365: 243-252.
- [71] Schatz A K, Scholten T, Kühn P. Paleoclimate and weathering of the Tokaj (Hungary) loess-paleosol sequence[J]. Palaeogeography, Palaeoclimatology, Palaeoecology, 2015, 426: 170-182.
- [72] Berra F, Jadoul F, Anelli A. Environmental control on the end of the Dolomia Principale/Hauptdolomit depositional system in the central Alps: Coupling sea-level and climate changes[J]. Palaeogeography, Palaeoclimatology, Palaeoecology, 2010, 290(1/2/3/4): 138-150.
- [73] Berra F. Sea-level fall, carbonate production, rainy days: How do they relate? Insight from Triassic carbonate platforms (western Tethys, southern Alps, Italy) [J]. Geology, 2012, 40(3): 271-274.
- [74] Schaller M F, Wright J D, Kent D V. A 30 Myr record of Late Triassic atmospheric pCO_2 variation reflects a fundamental control of the carbon cycle by changes in continental weathering[J]. Geological Society of America Bulletin, 2015, 127(5/6): 661-671.
- [75] Zaffani M, Agnini C, Concheri G, et al. The Norian “chaotic carbon interval”: New clues from the $\delta^{13}C_{org}$ record of the Lagonegro Basin (southern Italy) [J]. Geosphere, 2017, 13(4): 1133-1148.
- [76] Ernst R E, Buchan K L. The use of mafic dike swarms in identifying and locating mantle plumes[J]. Geological Society of America Special Papers, 2001, 352: 247-265.
- [77] Haq B U. Triassic eustatic variations reexamined[J]. GSA Today, 2018, 28(12): 4-9.
- [78] Sun Y D, Orchard M J, Kocsis Á T, et al. Carnian-Norian (Late Triassic) climate change: Evidence from conodont oxygen isotope thermometry with implications for reef development and Wrangellian tectonics[J]. Earth and Planetary Science Letters, 2020, 534: 116082.
- [79] Van Konijnenburg-Van Cittert J H A. Ecology of some Late Triassic to Early Cretaceous ferns in Eurasia[J]. Review of Palaeobotany and Palynology, 2002, 119(1/2): 113-124.
- [80] Abbink O A. Palynological investigations in the Jurassic of the North Sea region[M]. LPP Foundation, 1998: 192.
- [81] Philippe M, Thevenard F. Distribution and palaeoecology of the Mesozoic wood genus *Xenoxyylon*: Palaeoclimatological implications for the Jurassic of western Europe[J]. Review of Palaeobotany and Palynology, 1996, 91(1/2/3/4): 353-370.
- [82] Amiot R, Wang X, Zhou Z H, et al. Oxygen isotopes of East Asian dinosaurs reveal exceptionally cold Early Cretaceous climates[J]. Proceedings of the National Academy of Sciences of the United States of America, 2011, 108(13): 5179-5183.
- [83] Olsen P E, Kent D V. Milankovitch climate forcing in the tropics of Pangaea during the Late Triassic[J]. Palaeogeography, Palaeoclimatology, Palaeoecology, 1996, 122(1/2/3/4): 1-26.
- [84] Kent D V, Olsen P E. Magnetic polarity stratigraphy and paleolatitude of the Triassic-Jurassic Blomidon Formation in the Fundy Basin (Canada): Implications for Early Mesozoic tropical climate gradients[J]. Earth and Planetary Science Letters, 2000, 179(2): 311-324.
- [85] Kutzbach J E, Gallimore R G. Pangaea climates: Megamonsoons of the megacontinent[J]. Journal of Geophysical Research, 1989, 94(D3): 3341-3357.
- [86] de Wever P, O'Dogherty L, Goričan Š. Monsoon as a cause of radiolarite in the Tethyan realm[J]. Comptes Rendus Geoscience, 2014, 346(11/12): 287-297.
- [87] Pole M, Wang Y D, Dong C, et al. Fires and storms: A Triassic-Jurassic transition section in the Sichuan Basin, China[J]. Palaeobiodiversity and Palaeoenvironments, 2018, 98(1): 29-47.
- [88] Tanner L H. Climates of the Late Triassic: Perspectives, proxies and problems[M]//Tanner L H. The Late Triassic world: Earth in a time of transition. Cham: Springer International Publishing, 2018: 59-90.
- [89] Song Y, Algeo T J, Wu W J, et al. Distribution of pyrolytic PAHs across the Triassic-Jurassic boundary in the Sichuan Basin, southwestern China: Evidence of wildfire outside the central Atlantic magmatic province[J]. Earth-Science Reviews, 2020, 201: 102970.
- [90] 徐兆辉, 汪泽成, 胡素云, 等. 四川盆地上三叠统须家河组沉积时期古气候[J]. 古地理学报, 2010, 12(4): 415-424. [Xu Zhaozhi, Wang Zecheng, Hu Suyun, et al. Paleoclimate during depositional period of the Upper Triassic Xujiahe Formation in Sichuan Basin[J]. Journal of Palaeogeography, 2010, 12(4): 415-424.]
- [91] Preto N, Kustatscher E, Wignall P B. Triassic climates: State of the art and perspectives[J]. Palaeogeography, Palaeoclimatology,

- Palaeoecology, 2010, 290(1/2/3/4): 1-10.
- [92] 钱利军,时志强,李智武,等. 四川盆地西缘地区上三叠统须家河组化石木年轮的古气候意义[J]. 沉积学报,2010,28(2): 324-330. [Qian Lijun, Shi Zhiqiang, Li Zhiwu, et al. Fossil wood of the Upper Triassic Xujiahe Formation on the western margin of Sichuan Basin: Implication for palaeoclimate[J]. *Acta Sedimentologica Sinica*, 2010, 28(2): 324-330.]
- [93] Haas J, Demény A. Early dolomitisation of Late Triassic platform carbonates in the Transdanubian range (Hungary)[J]. *Sedimentary Geology*, 2002, 151(3/4): 225-242.
- [94] Ahlberg A, Arndorff L, Guy-Ochluss D. Onshore climate change during the Late Triassic marine inundation of the Central European Basin[J]. *Terra Nova*, 2002, 14(4): 241-248.
- [95] Cesar J, Grice K. Molecular fingerprint from plant biomarkers in Triassic-Jurassic petroleum source rocks from the Dampier sub-basin, northwest shelf of Australia[J]. *Marine and Petroleum Geology*, 2019, 110: 189-197.
- [96] Therrien F, Fastovsky D E. Paleoenvironments of Early Theropods, Chinle Formation (Late Triassic), Petrified Forest National Park, Arizona[J]. *Palaios*, 2000, 15(3): 194-211.
- [97] Nakada R, Ogawa K, Suzuki N, et al. Late Triassic compositional changes of aeolian dusts in the pelagic Panthalassa: Response to the continental climatic change[J]. *Palaeogeography, Palaeoclimatology, Palaeoecology*, 2014, 393: 61-75.
- [98] 胡修棉,李娟,韩中,等. 中新生代两类极热事件的环境变化、生态效应与驱动机制[J]. 中国科学(D辑):地球科学,2020,50(8): 1023-1043. [Hu Xiumian, Li Juan, Han Zhong, et al. Two types of hyperthermal events in the Mesozoic-Cenozoic: Environmental impacts, biotic effects, and driving mechanisms[J]. *Science China (Seri. D): Earth Sciences*, 2020, 50(8): 1023-1043.]
- [99] Shen S Z, Ramezani J, Chen J, et al. A sudden end-Permian mass extinction in South China[J]. *GSA Bulletin*, 2019, 131(1/2): 205-223.
- [100] Sun Y D, Joachimski M M, Wignall P B, et al. Lethally hot temperatures during the Early Triassic greenhouse[J]. *Science*, 2012, 338(6105): 366-370.
- [101] Kuroda J, Hori R S, Suzuki K, et al. Marine osmium isotope record across the Triassic-Jurassic boundary from a Pacific pelagic site[J]. *Geology*, 2010, 38(12): 1095-1098.
- [102] Nozaki T, Nikaido T, Onoue T, et al. Triassic marine Os isotope record from a pelagic chert succession, Sakahogi section, Mino Belt, southwest Japan[J]. *Journal of Asian Earth Sciences*: X, 2019, 1: 100004.
- [103] Zaffani M, Jadoul F, Rigo M. A new Rhaetian $\delta^{13}\text{C}_{\text{org}}$ record: Carbon cycle disturbances, volcanism, End-Triassic mass Extinction (ETE)[J]. *Earth-Science Reviews*, 2018, 178: 92-104.
- [104] 杨博. 新疆准噶尔盆地东部侏罗世煤中古野火事件及其气候指示意义[D]. 乌鲁木齐:新疆大学,2021. [Yang Bo. Paleowildfire events and its climatic implications in Middle Jurassic coal seams in eastern Junggar Basin, Xinjiang[D]. Urumqi: Xinjiang University, 2021.]
- [105] Ziegler A, Eshel G, Rees P M, et al. Tracing the tropics across land and sea: Permian to present[J]. *Lethaia*, 2003, 36(3): 227-254.
- [106] Tanner L H, Lucas S G. Stratigraphic distribution and significance of a 15 million-year record of fusain in the Upper Triassic Chinle Group, southwestern USA[J]. *Palaeogeography, Palaeoclimatology, Palaeoecology*, 2016, 461: 261-271.
- [107] Byers B A, Ash S R, Chaney D, et al. First known fire scar on a fossil tree trunk provides evidence of Late Triassic wildfire [J]. *Palaeogeography, Palaeoclimatology, Palaeoecology*, 2014, 411: 180-187.
- [108] Uhl D, Montenari M. Charcoal as evidence of palaeo-wildfires in the Late Triassic of SW Germany[J]. *Geological Journal*, 2011, 46(1): 34-41.
- [109] Petersen H I, Lindström S. Synchronous wildfire activity rise and mire deforestation at the Triassic-Jurassic boundary[J]. *PLoS One*, 2012, 7(10): e47236.
- [110] Marynowski L, Simoneit B R T. Widespread Upper Triassic to Lower Jurassic wildfire records from Poland: Evidence from charcoal and pyrolytic polycyclic aromatic hydrocarbons[J]. *Palaios*, 2009, 24(12): 785-798.

Paleoclimate Perturbation and Its Driving Mechanism Across Norian-Rhaetian Transition (Late Triassic) in the Xujiahe Formation, Sichuan Basin

CHEN YuChao¹, JIN Xin^{1,2,3}, DU YiXing^{1,2}, ZHANG YunWang¹, LI BinBing¹, SHI ZhiQiang^{1,2}

1. Institute of Sedimentary Geology, Chengdu University of Technology, Chengdu 610059, China

2. State Key Laboratory of Oil and Gas Reservoir Geology and Exploitation, Chengdu University of Technology, Chengdu 610059, China

3. State Key Laboratory of Loess and Quaternary Geology, Institute of Earth Environment, Chinese Academy of Sciences, Xi'an 710061, China

Abstract: [Objective] The paleoclimate and environment have changed significantly across the Norian-Rhaetian transition (NRT, Late Triassic), as demonstrated by carbon-isotope fluctuations and biological extinction events.

However, the causes of climate perturbations and biotic crises during the NRT remain controversial. It is believed that the eruption of contemporaneous volcanisms (e.g., the Angayucham Large Igneous Province) was the main cause of paleoenvironmental changes during the NRT. The large-scale volcanic activity released a large amount of greenhouse gases, which resulted in global temperature rise, carbon-isotope perturbation, and biological crises during the NRT. At present, the majority of NRT studies have focused on the shallow marine strata in the Tethys region, but knowledge on the changes in terrestrial paleoclimate, paleoenvironment, and their driving mechanism during the NRT is extremely limited. Studies have shown that terrestrial strata can faithfully record paleoclimatic and paleoenvironmental changes during geological events, such as the end-Permian mass extinction. However, previous studies mainly focused on paleobotany, sedimentology, organic carbon isotopes, and wildfires during the NRT in the Sichuan Basin, but lacked element geochemical evidence, limiting the accurate understanding of the climatic changes in this time interval and the comparison between different research methods. [Methods] To tackle this scientific question, we examined the Norian-Rhaetian section (Xujiahe section) located 4.5 km NE of Guangyuan city, northwest Sichuan Basin. Thirty-four samples were collected at a resolution of 10 cm to 2 m in the Xujiahe section for major and trace element compositions. The surface dust and weathered portions of samples were removed with a rasper and then washed with deionized water. After 8 hours of oven drying at 50 °C, samples were ground into powder using agate mortars. Sample preparations were completed in the School of Materials and Chemistry & Chemical Engineering, Chengdu University of Technology. Analysis of major and trace elements in samples was completed at the Institute of Earth Environment, Chinese Academy of Sciences, Xi 'an. A glass bead was created by fusing 0.6 g of the powdered sample with 6 g of dry lithium tetraborate ($\text{Li}_2\text{B}_4\text{O}_7$) for 5 minutes at 1 000 °C. The glass bead was further scanned by an X-ray fluorescence spectrometer (WD-XRF; PANalytical, Ea Almelo, The Netherlands). The analytical accuracy was better than 2%. [Results and Discussions] The analyzed samples have high Chemical Index of Alteration (CIA) values and Rb/Sr at 105.5, 110.2-122.5, 119, 123.4-123.45, and 137.7 m in the Xujiahe section, and low CIA values and Rb/Sr at 107, 109.5, 115.5-116.5, 121.5, and 127-135m. The uppermost part of Upper Norian successions (105.5-129.5m) have CIA values ranging from 59 to 82, with a mean of 73; Rb/Sr values ranging from 0.2 to 2.6, with a mean of 1.2; and R values ranging from 3.8 to 16.9, with a mean of 8.2. For the Norian-Rhaetian boundary interval (NRB, 129.5-135 m), CIA values range from 59 to 63, with a mean of 60; Rb/Sr values range from 0.5 to 0.6, with a mean of 0.5; and R values range from 13.1 to 13.9, with a mean of 13.5. [Conclusions] Results show that the climate fluctuated frequently during the NRT of Xujiahe section in the Sichuan Basin. The Late Norian was dominated by warm and humid climate, which was interrupted by a short-term cooling event close to the NRB. The prevailing mega-monsoon in Pangaea during the Late Triassic may be the main trigger for the frequent climate change and NRB cooling events in the Xujiahe section, but the influence of volcanic activity and wildfire events on the paleoclimate system cannot be eliminated in this time period. To determine the precise timing of volcanic eruptions and wildfires during the NRT and how they contributed to climate change, more research is needed.

Key words: Late Triassic; Xujiahe Formation; paleoclimate; weathering index; Sichuan Basin